Original Article

MOLECULAR METABOLISM

PDK1-Foxo1 pathway in AgRP neurons of arcuate nucleus promotes bone formation via GHRH-GH-IGF1 axis

Hideyuki Sasanuma [1,2], Masanori Nakata [1,], Kumari Parmila [1], Jun Nakae [3], Toshihiko Yada [1,*]**

ABSTRACT

Objective: In the hypothalamic arcuate nucleus (ARC), orexigenic agouti-related peptide (AgRP) neurons regulate feeding behavior and energy homeostasis, functions connected to bone metabolism. The 3-phosphoinositide-dependent protein kinase-1 (PDK1) serves as a major signaling molecule particularly for leptin and insulin in AgRP neurons. We asked whether PDK1 in AGRP neurons also contributes to bone metabolism.
Methods: We generated AgRP neuron-specific PDK1 knockout (*Agrp Pdk1*$^{-/-}$) mice and those with additional AgRP neuron-specific expression of transactivation-defective FoxO1 (*Agrp Pdk1*$^{-/-}$ *Δ256Foxo1*). Bone metabolism in KO and WT mice was analyzed by quantitative computed tomography (QCT), bone histomorphometry, measurement of plasma biomarkers, and qPCR analysis of peptides.
Results: In *Agrp Pdk1*$^{-/-}$ female mice aged 6 weeks, compared with *Agrp* Cre mice, both stature and femur length were shorter while body weight was unchanged. Cortical bone mineral density (BMD) and cancellous BMD in the femur decreased, and bone formation was delayed. Furthermore, plasma GH and IGF-1 levels were reduced in parallel with decreased mRNA expressions for GH in pituitary and GHRH in ARC. Osteoblast activity was suppressed and osteoclast activity was enhanced. These changes in stature, BMD and GH level were rescued in *Agrp Pdk1*$^{-/-}$ *Δ256Foxo1* mice, suggesting that the bone abnormalities and impaired GH release were mediated by enhanced Foxo1 due to deletion of PDK1.
Conclusions: This study reveals a novel role of PDK1-Foxo1 pathway of AgRP neurons in controlling bone metabolism primarily via GHRH-GH-IGF-1 axis.

Keywords AgRP; GHRH; Growth hormone; PDK1; Foxo1; Bone mineralization

1. INTRODUCTION

It has recently been recognized that obesity causes the complication of bone metabolism associated with metabolic syndrome [1]. It has been shown that bone metabolism is related to energy metabolism and regulated substantially by the central nervous system [2–5]. Agouti-related protein (AgRP) neurons co-expressing neuropeptide Y (NPY) are localized specifically in the medial section of hypothalamic arcuate nucleus (ARC) and play an essential role in promoting food consumption and suppressing energy expenditure [6–11]. Recently, it was shown that the neural activity of AgRP neurons plays a role in bone metabolism [12].
Insulin acts on the ARC AgRP/NPY neurons via a signaling cascade that suppresses food consumption [13,14]. Activation of insulin receptors, as well as insulin-like growth factor (IGF-1) receptors, phosphorylates the insulin receptor substrate (IRS) and activates phosphatidylinositol-3 kinase (PI3K) to generate phosphatidylinositol-3, 4, 5-trisphosphate (PIP3) and phosphatidylinositol-4, 5-bisphosphate (PIP2). PIP3 activates 3-phosphoinositide-dependent protein kinase 1 (PDK1), which, in turn, activates protein kinase B (PKB, also known as Akt) and members of the atypical PKC family. Subsequently, PKB targets the forkhead transcription factor, forkhead box O (FoxO) [15].
FoxO is defined by its N-terminal forkhead DNA binding domain and C-terminal trans-activation domain [15]. FoxO proteins are the most divergent subfamily of forkhead proteins, based on homologies within the DNA-binding domain. Invertebrates have a FoxO gene, Drosophila have dFOXO, Caenorhabditis elegans have DAF-16, and mammals have FoxO1 (FKHR), FoxO3 (FKHRL1), FoxO4 (AFX), and FoxO6 [15]. Among them, FoxO1 plays a pivotal role in mediating the effects of insulin and IGF1 on the expression of genes involved in cell growth, differentiation, metabolism, and longevity [16–20].

[1]Department of Physiology, Division of Integrative Physiology, Jichi Medical University, 3311-1 Yakushiji, Tochigi, Shimotsuke, 329-0498, Japan [2]Department of Orthopaedic Surgery, Faculty of Medicine, Jichi Medical University, 3311-1 Yakushiji, Tochigi, Shimotsuke, 329-0498, Japan [3]Frontier Medicine on Metabolic Syndrome, Division of Endocrinology, Metabolism and Nephrology, Department of Internal Medicine, Keio University School of Medicine, Tokyo, Japan

*Corresponding author. Fax: +81 285 44 9962. E-mail: tyada@jichi.ac.jp (T. Yada).

**Corresponding author. Fax: +81 285 44 9962. E-mail: nakata@jichi.ac.jp (M. Nakata).

Abbreviations: PVN, paraventricular nucleus; GHRH, Growth hormone releasing hormone; IGF-1, insulin-like growth factor-1; ARC, arcuate; BMD, bone mineral density

Received February 1, 2017 • Accepted February 11, 2017 • Available online 17 February 2017

http://dx.doi.org/10.1016/j.molmet.2017.02.003

In response to insulin and IGF-1, FoxO1 is phosphorylated at three highly conserved phosphorylation sites (Thr24, Ser253 and Ser316) through the PI3K-dependent pathway, resulting in its nuclear exclusion and inhibition of target gene expression [16,17]. Failure to phosphorylate of FoxO1 results in its permanent nuclear localization and constitutive transactivation of gene expression.

We previously reported that the PDK1-FoxO1 pathway in AgRP neurons regulates food consumption and energy metabolism [21]. However, its relationship to bone metabolism remains unknown. It was reported that injection of AgRP targeting antisense Morpholino oligonucleotides acutely suppresses somatic growth in larval teleosts [22] and that hypothalamic NPY is implicated in bone metabolism in rodents [23]. The interaction between ARC AgRP/NPY neurons and GHRH neurons and periventricular nucleus somatostatin neurons via NPY Y1 and Y2 receptors has been reported [24]. Thus, AgRP/NPY neurons in the ARC might be involved in bone metabolism. This study aimed to explore the role of AgRP neurons, particularly PDK1 and FoxO1 in these neurons, in bone metabolism by analyzing AgRP neuron-specific PDK1 knockout mice (*Agrp Pdk1*$^{-/-}$) and those with additional expression of transactivation-defective FoxO1 (*Agrp Pdk1*$^{-/-}$ *Δ256Foxo1*) [21].

2. SUBJECTS AND METHODS

2.1. AgRP neuron-specific PDK1 knockout mice (*Agrp PDK1*$^{flox/flox}$) and Δ256FoxO1-transgenic and PDK1 knockout mice (*Agrp PDK1*$^{flox/flox}$ *Δ256Foxo1*)

We generated AgRP neuron-specific PDK1 knockout mice [21] by mating AgRP-Cre-transgenic (Agrp Cre) mice [25] with PDK1$^{flox/flox}$ mice with loxP sites flanking exons 3 and 4 [26]. AgRP neuron-specific Δ256FoxO1-transgenic mice were generated by mating R26$^{flox\text{-}neo\Delta256Foxo1}$ mice [27] with Agrp Cre mice. Moreover, Δ256FoxO1-transgenic and PDK1 knockout mice (*Agrp PDK1*$^{flox/flox}$ *Δ256Foxo1*) were generated by mating Agrp PDK1$^{flox/flox}$ mice with AgRP neuron-specific Δ256FoxO1-transgenic mice as previously described [21]. All mice were genotyped by polymerase chain reaction (PCR) amplification of genomic DNA isolated from tail tips. Mice were maintained under on 12 h light/dark cycle (7:30 lights on) and given standard food CE-2 (Japan SLC, Tokyo, Japan) and water ad libitum. For feeding experiment, mice were housed individually. All experimental protocols were approved by the Jichi Medical University Institute of Animal Care and Use Committee.

2.2. Measurement of naso-anal length and femur length

We used 6 and 15 week old female mice. Immediately after the animals were euthanized, left femurs were removed and dissected free of soft tissue. Naso-anal lengths and femur lengths were measured using a micrometer caliper. X-ray radiographs of total left femurs were taken by the X-ray system (LaTheta LCT-200S; Aloka, Tokyo, Japan). We defined the femur length as a longitudinal distance from tip of the great trochanter to the center of the femoral condyle.

2.3. Peripheral quantitative computed tomography (pQCT) analysis

Left femurs of 6 and 15 week old female mice were used for the pQCT analysis. We used pQCT with a fixed x-ray fan beam of 10-mm spot size, at 1 mA and 50 kVp (LaTheta LCT-200S; Aloka, Tokyo, Japan). About 300 slices (240 × 240-pixel matrix per slice, 0.1 mm thickness, a voxel size of 48 × 48 μm^2) covered the entire left femur and were recreated to the 3D CT picture of an axial view of the distal femur by using the VGStudio MAX1.2 software (Nihon Visual Science, Tokyo, Japan).

To measure the bone mineral density (BMD) and strength of bones at the left femur from each mouse, the regions of interest (ROI) was defined as range from the tip of the great trochanteric part to the part of distal condyle. We measured cortical bone mineral density (BMD), cancellous BMD, total BMD, minimum moment of inertia of area, and polar moment of inertia of area.

2.4. Bone histomorphometry

For dynamic histomorphometric analysis of bone formation, all animals were labeled with calcein. At 1 and 6 days before euthanasia, calcein (Sigma, St Louis, MO, USA) was administered subcutaneously at a dose of 8 mg/g of BW. Right femurs of 6 week old female mice were stripped of all muscles and immediately fixed in 70% ethanol, embedded in methyl methacrylate without decalcification, and stained with Villanueva bone stain. Coronal sections of the distal portion of the femur were cut to respective thickness of 20 μm using a microgrinding machine (KG4000; Exakt-Apparatebau, Norderstedt, Germany). Histomorphometrical analysis was performed as in [28,29]. Briefly, the region of the distal femur metaphysis 1−4 mm proximal to the growth plate metaphyseal junction was examined. All parameters were calculated according to the recommendations of the Histomorphometry Nomenclature Committee of the American Society of Bone and Mineral Research [30]. The width of epiphyseal growth plate was measured.

2.5. Measurement of plasma biomarkers for bone metabolism

At 6 weeks of age, the blood was collected at 12:00 (noon). Bone Specific Alkaline Phosphatase (BAP) and tartrate-resistant acid phosphatase 5b (TRACP-5b) were measured using a specific enzyme immunoassay (CUSABIO BIOTECH, Ltd, Wuhan, China). The receptor activator of NF-κB ligand (RANKL) was measured using ELISA kit (R&D SYSTEMS, Minneapolis, MN, USA). Osteocalcin was measured using a MOUSE OSTEOCALCIN EIA KIT (Biomedical Tec Inc., Stoughton, MA, USA). Serum Ca level was measured using a calcium E-test WAKO (WAKO, Tokyo, Japan). β-estradiol (E2) was measured using an Estradiol EIA Kit (Cayman Chemical Co., Ann Arbor, MI, USA). IGF-1 was measured using an Assay Max Mouse IGF-1 ELISA Kit (ASSAYPRO, St. Charles, MO, USA). Growth hormone (GH) was measured using a Rat/Mouse Growth Hormone ELISA kit (MILLIPORE, Billerica, MA, USA). Insulin was measured using a sensitive mouse insulin ELISA kit (Shibayagi, Gumma, Japan).

2.6. Immunohistochemistry

For immunohistochemical analyses, mice were perfused transcardially with heparinized saline (heparin 20 unit/ml), followed by 4% paraformaldehyde (PFA) in 0.1 M phosphate-buffered saline at pH 7.4 (PBS). The brains and pituitaries were dissected and immersed in 4% paraformaldehyde at 4 °C overnight. They were embedded in paraffin, and coronal sections were cut into respective thicknesses of 5 μm using a microtome (Carl Zeiss Co., Ltd, Germany). After deparaffinization, the sections were washed in PBS and immersed in 0.3% H_2O_2/PBS for 10 min for endogenous peroxidase blocking. Then, blocking was performed in 1% bovine serum albumin for 30 min. For GH immunostaining in the pituitary, sections were first incubated with goat anti-rat GH antibody (dilution 1: 200) (R&D Systems, Minneapolis, MN, USA) for 3 h followed by incubation with biotinylated horse anti-goat IgG antibody (dilution 1: 800) (Vector, CA, USA) for 60 min. Sections were incubated in a DAB solution (Sigma, St. Louis, MO, USA) for 5 min to develop the color reaction. Observation was performed with an AX80TR light microscope (Olympus, Tokyo, Japan). For growth hormone-releasing hormone (GHRH) staining in hypothalamus, sections were incubated first with rabbit anti- GHRH antibody (ab187512, dilution 1:200) (Abcam, Cambridge, UK) and subsequently with Alexa fluor 488 goat anti-rabbit (Life Technologies, Carlsbad, CA; 1:1000).

The confocal fluorescence images for GHRH were acquired using Olympus FV1000 confocal laser-scanning microscope (Olympus, Tokyo, Japan). The fluorescence intensity of GHRH in median eminence was quantified by ImageJ (NIH).

2.7. Real-time RT-PCR analysis

Transverse brain slices were prepared from 6 week old mice. A 1 mm coronal brain slice containing arcuate, orientated by median eminence and optic chiasm, was prepared using a Precision Brain Slicer (Braintree Scientific, Inc). A block of tissue containing both sides of arcuate was dissected from the slice with a scalpel under stereoscopic microscope (SMZ645, Nikon, Japan). Total RNA was isolated from the hypothalamus and pituitary using TRIzol reagent (Invitrogen, Carlsbad, CA, USA) and was treated with RQ1-DNase (Promega, Madison, WI, USA) to remove residual DNA contamination. First-strand cDNA synthesis was performed using ReverTra Ace (TOYOBO Co, Japan). After conversion to cDNA, real-time RT-PCR was performed with SYBR premix Ex taq II polymerase (Takara Bio, Tokyo, Japan) (95 °C for 5 s and 60 °C for 30 s × 40 cycles) in Thermal Cycler Dice Real Time System TP800 2.10B (Takara Bio). Product accumulation was measured in real time, and the mean cycle threshold (Ct; the cycle during which product is first detected) was determined for replicate samples run on the same plate. The comparative method of relative quantification was used to calculate the expression level of GH and GHRH genes, normalized to housekeeping gene, glyceraldehyde-3-phosphate dehydrogenase (GAPDH). Expression levels of mRNAs were calculated by the 2ΔΔCT method of relative quantification, and normalized to housekeeping gene products GAPDH.

2.8. Primers were as follows

GAPDH: 5′-GGCACAGTCAAGGCTGAGAATG-3′ and 5′-ATGGTGGTGAAGACGCCAGTA-3′,
GHRH: 5′-TGCCATCTTCACCACCAAC-3′ and 5′-TCATCTGCTTGTCCTCTGTCC-3′,
GH: 5′- CCTCAGCAGGATTTTCACCA-3′ and 5′-CTTGAGGATCTGCCCAACAC-3′.

2.9. Western blot analysis

At 6 weeks of age, the pituitary gland and median eminence were removed from mice after transcardial perfusion with heparinized saline (heparin 20 unit/ml). The tissues were lysed in 40 μl lysis buffer [100 mM NaCl, 0.5% NP40, 1 mM EDTA, 10 mM Tris—HCl (pH 7.5), 0.5 U aprotinin, and 1 mM PMSF]. NP-40 lysates were centrifuged at 12,000 g for 10 min at 4 °C. The supernatants were eluted in Laemmli's SDS—PAGE sample buffer containing 1% SDS and 5% 2-mercaptoethanol. The 1 μg proteins were subjected to 15% SDS—PAGE and transferred to nitrocellulose filters. Growth hormone (R&D, 1:5000) was detected with the polyclonal antibody. Immunoreactive proteins were detected with HRP-conjugated secondary antibody and the ECL system (Amersham Corp., Arlington Heights, IL). After striping, membrane was hybridized with anti-rat syntaxin1 antibody (Carbiochem, San Diego, CA 1:2000). Immunoreactive signal was quantified by FAS-1000 (Fujifilm, Japan), and signal levels of GH were normalized to syntaxin 1.

2.10. Urine collections

At 6 weeks of age, urine samples were collected during a 24 h period with the mouse metabolic cage CM-10S (CLEA Japan Co. Ltd., Tokyo, Japan). Urinary norepinephrine concentration was determined with high performance liquid chromatography (SRL).

2.11. Statistical analysis

Data are expressed as means ± s.e.m. Data were analyzed for statistical significance by two-tailed unpaired Student's t test for two groups and one-way ANOVA followed by a Bonferroni's multiple comparison test for multiple groups. $P < 0.05$ was considered significant.

3. RESULTS

3.1. *Agrp Pdk1*$^{-/-}$ mice show short stature, short femur length, reduced bone mass, and impaired bone strength

Naso-anal lengths were significantly shorter in female *Agrp Pdk1*$^{-/-}$ mice aged 6 and 15 weeks compared to *Agrp Cre* mice (Figure 1A). Naso-anal lengths were also shorter in male *Agrp Pdk1*$^{-/-}$ mice to a lesser extent (Figure 1B). Food intake in male *Agrp Pdk1*$^{-/-}$ mice tended to decrease compared to male *Agrp Cre* mice (Cre 3.188 ± 0.109 vs. KO 2.884 ± 0.109, $P = 0.08$), while no difference in food intake was observed between female *Agrp Cre* mice and *Agrp Pdk1*$^{-/-}$ mice (Cre 2.757 ± 0.077 vs. KO 2.623 ± 0.046). In contrast, the retardation of skeletal growth was remarkable in female *Agrp* Pdk1$^{-/-}$ mice. Hence, to observe the direct effect on growth independent of that on food intake, female mice were analyzed in the rest of the study unless otherwise stated. The radiographs of the left femur demonstrated shorter length in *Agrp Pdk1*$^{-/-}$ mice at 6 weeks (Figure 1C). The average femur lengths were significantly shorter at both 6 and 15 weeks of age in *Agrp Pdk1*$^{-/-}$ mice compared to *Agrp Cre* mice (Figure 1D). Next, pQCT analysis was performed for the left femur of mice aged 6 and 15 weeks. A 3D-CT picture of the axial view of the distal femur demonstrated that the bone width of the cortical bone was narrower and the cancellous bone mass was lower in *Agrp Pdk1*$^{-/-}$ than in *Agrp Cre* mice (Figure 1E). At 6 weeks of age, cortical bone mineral density (BMD), cancellous BMD, and total BMD, which are indicators of bone strength, all decreased significantly in *Agrp Pdk1*$^{-/-}$ *mice* (Figure 1F—H). At 15 weeks, cancellous BMD and total BMD were also significantly lower in *Agrp Pdk1*$^{-/-}$ mice. In *Agrp Pdk1*$^{-/-}$ mice at both 6 and 15 weeks of age, cortical BMD was reduced by approximately 7% and cancellous BMD by approximately 20% compared with *Agrp Cre* mice. Thus, the decrease in bone density was more pronounced for the cancellous bone. Both the minimum moment of inertia of area representing breaking strength and the polar moment of inertial area representing torsional strength decreased significantly in *Agrp Pdk1*$^{-/-}$ mice at 6 and 15 weeks of age (Figure 1I,J).

3.2. *Agrp Pdk1*$^{-/-}$ mice show reduced bone formation and altered bone metabolism markers

Histomorphometric analysis of the cancellous bone of right femur demonstrated a significant decrease in bone mass in 6 week old *Agrp Pdk1*$^{-/-}$ mice (Figure 2A,B). The width of bone trabeculae, osteoblast surface, osteoid surface, and osteoid area decreased in *Agrp Pdk1*$^{-/-}$ mice (Figure 2C). Regarding the bone resorption parameters, the number of osteoclasts and the osteoclastic surface tended to increase though these changes were not statistically significant, and the bone resorption surface significantly increased, compared with *Agrp Cre* mice (Figure 2D). Furthermore, Calcein double labeling showed that the width between the two stained labels was narrower in *Agrp Pdk1*$^{-/-}$ (Figure 2 E), indicating that the velocity of bone formation significantly decreased (Figure 2F). The width of the accretion line tended to decrease in *Agrp Pdk1*$^{-/-}$ mice, though the change was not statistically significant (Figure 2G,H, $p = 0.098$).

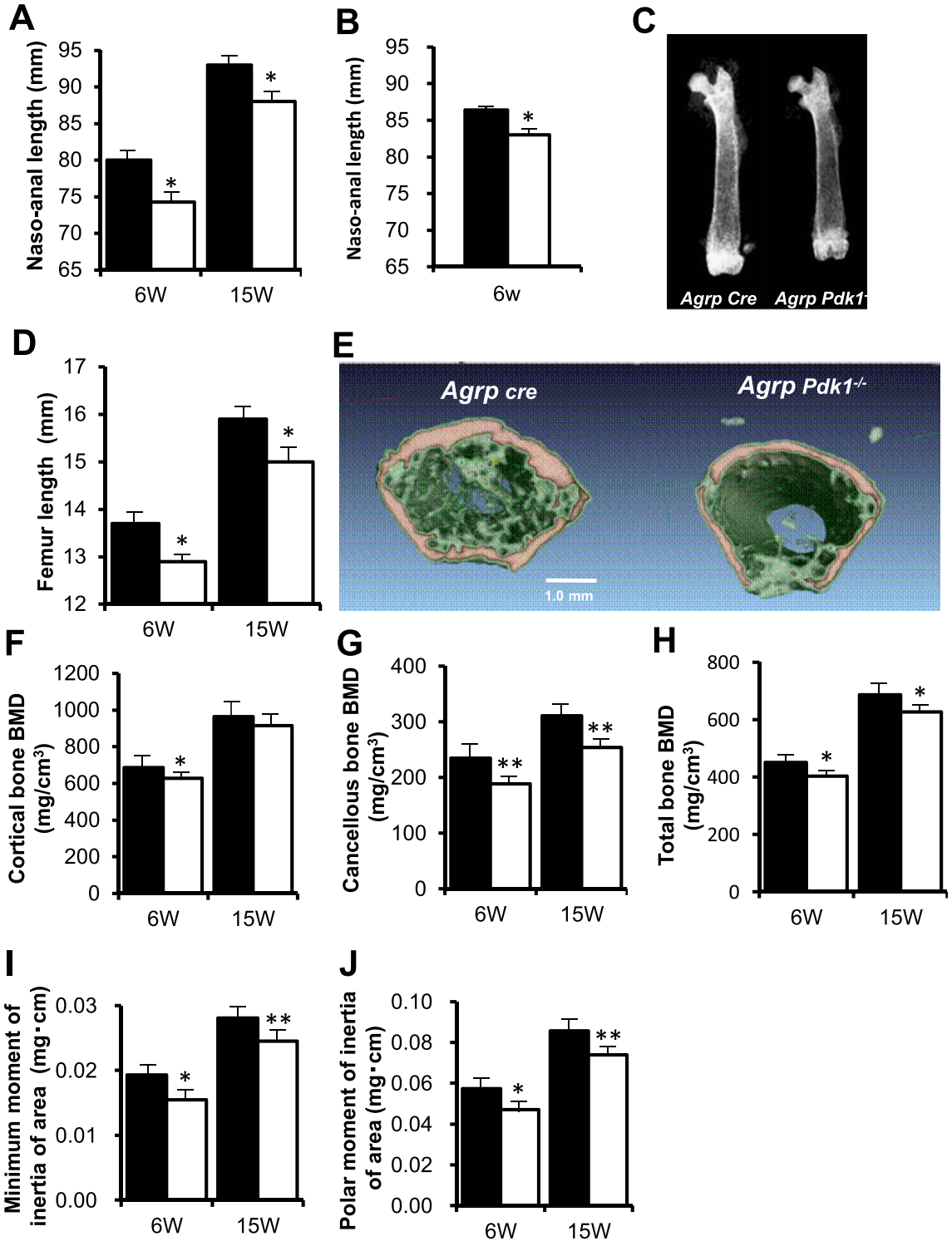

Figure 1: Decreased femur length, bone density, and strength in female *Agrp Pdk1*$^{-/-}$ mice aged 6 and 15 weeks. The pQCT and X-ray analysis of femur in female *Agrp Cre* (filled bars) and *Agrp Pdk1*$^{-/-}$ mice (open bars) at 6 and 15 weeks of age. **A and B**: Naso-anal length of female (A) and male (B). n = 7 per group. **C and D**: X-ray analysis of femurs at 6 weeks (C) and average femur lengths at 6 and 12 weeks of age (D) in female *Agrp Cre* and *Agrp Pdk1*$^{-/-}$ mice. n = 7 per group. **E**: 3DCT analysis of trabecular and cortical bone of distal femurs from 15 weeks old female mice. **F**: Cortical bone BMD. **G**: Cancellous bone BMD. **H**: Total bone BMD. **I**: Calculated Minimum moment of inertia of area. **J**: Calculated Polar moment of inertia of area. n = 10 per group in (D) to (I). $^{**}p < 0.01$, $^{*}p < 0.05$. ■, *Agrp Cre* mice; □, *Agrp Pdk1*$^{-/-}$ mice.

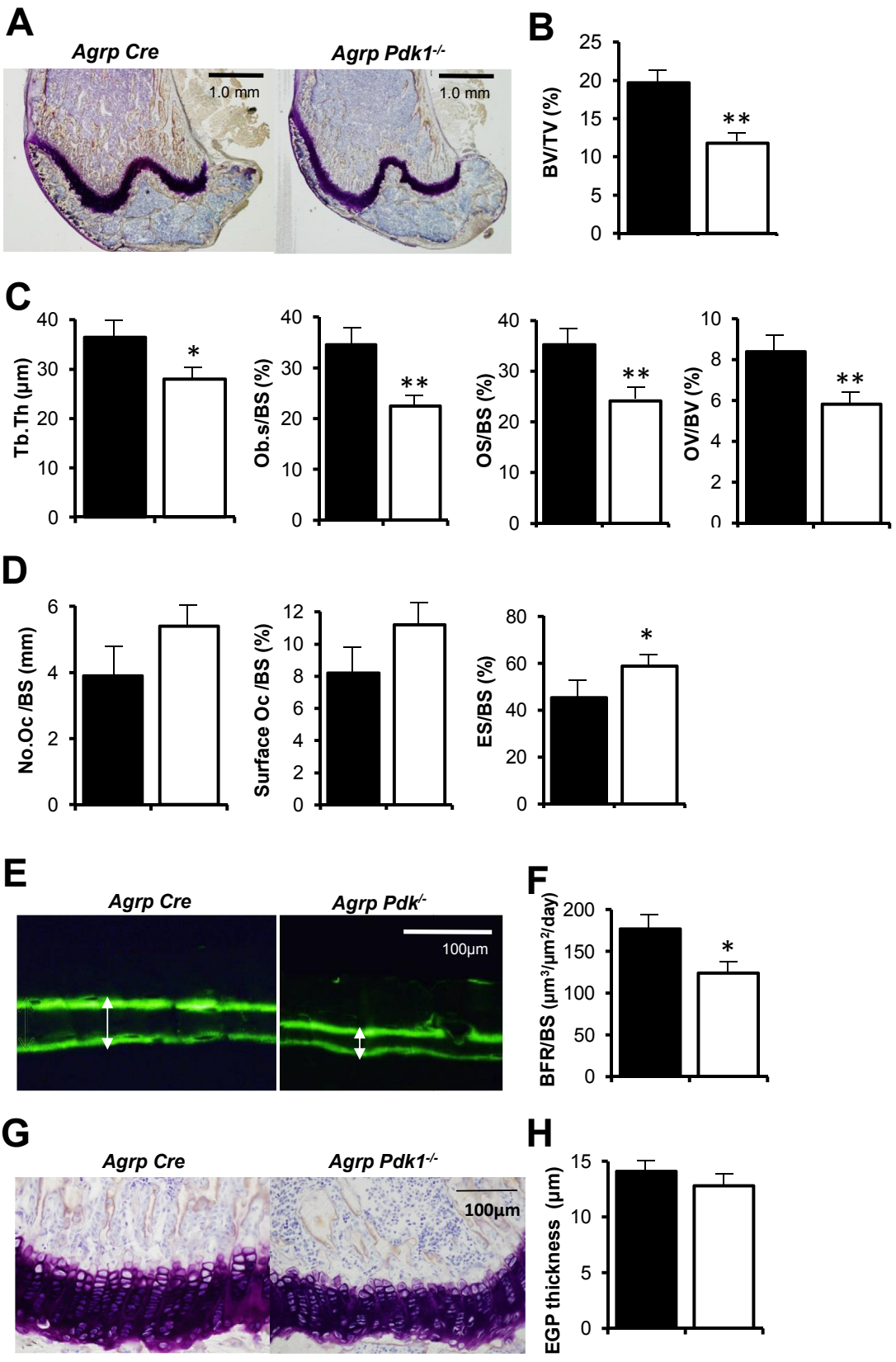

Figure 2: Lower bone mass due to decreased bone formation in 6 week old female *Agrp pdk1*$^{-/-}$ mice. A: Histologic section of undecalcified distal femur from 6 week old female *Agrp Cre* and *Agrp Pdk1*$^{-/-}$ mice, with Villanueva's bone staining. Bar = 1.0 mm. **B**: Bone volume per tissue volume (BV/TV). **C**: Trabecular thickness (Tb.Th), osteoblast surface area over bone surface area (Ob.s/BS), osteoid surface area over bone surface area (OS/BS), and osteoid volume per BV (OV/BV). **D**: Number of osteoclasts per bone surface (No. Oc/BS), osteoclast surface per bone surface (Oc.s/BS), and erosion surface area per bone surface area (ES/BS). **E**: Calcein double labeling. The distance between the two labels (arrow), representing the rate of bone formation, was significantly decreased in *Agrp Pdk1*$^{-/-}$ mice. Bar, 100 μm. **F**: Bone formation rate per bone surface (BFR/BS). **G**: Histologic section of epiphyseal growth plate. Bar, 100 μm. **H**: epiphyseal growth plate (EGP) thickness. n = 8 per group. $^{**}p < 0.01$, $^{*}p < 0.05$. ■, *Agrp Cre* mice; □, *Agrp Pdk1*$^{-/-}$ mice.

The bone histomorphometric analysis revealed that the cancellous bone tissue of the distal femur in *Agrp Pdk1*$^{-/-}$ mice showed the pattern of retardation of bone formation (Figure 2B, C, D and F). Thus, *Agrp Pdk1*$^{-/-}$ mice exhibited osteopenia with decreased osteoblastic bone formation and increased osteoclastic bone resorption.

These data showing reduced bone formation in *Agrp Pdk1*$^{-/-}$ mice prompted us to measure the bone metabolism markers. No significant difference was observed in the bone formation marker bone alkaline phosphatase (BAP) in *Agrp Pdk1*$^{-/-}$ mice (Figure 3A). In contrast, plasma concentration of the bone resorption markers TRACP5b and RANKL increased significantly in *Agrp Pdk1*$^{-/-}$ mice (Figure 3B,C), which was also consistent with the histomorphometric data showing enhanced bone resorption (Figure 2D). Plasma concentration of osteocalcin, a marker of bone mineralization, also decreased significantly (Figure 3D), consistent with the histomorphometric data showing reduced bone formation (Figure 2B, C and F).

3.3. *Agrp Pdk1*$^{-/-}$ mice show impaired GH-IGF-1 signaling

Plasma factors that influence bone metabolism were measured next. Plasma Ca^{2+}, estradiol, and insulin concentrations were not different between female *Agrp Pdk1*$^{-/-}$ and *Agrp Cre* mice at 6 weeks of age (Figure 4A, B and C). In contrast, plasma IGF-1 and GH concentrations decreased significantly in female *Agrp Pdk1*$^{-/-}$ mice (Figure 4D, E). In male *Agrp Pdk1*$^{-/-}$ mice, plasma GH also decreased, but to a lesser extent (Figure 4F). Based on these results, we investigated protein and mRNA expression for GH in the pituitary and for and its upstream stimulator GHRH in the pituitary and hypothalamus, respectively. Immunohistochemical analysis showed that the ratio of the number of GH-immunoreactive cells over total cells in unit area of the anterior pituitary was not altered in 6 week old female *Agrp Pdk1*$^{-/-}$ mice (Figure 5A, B). By contrast, mRNA and protein expression of GH in the pituitary markedly decreased in *Agrp Pdk1*$^{-/-}$ mice (Figure 5C, D). Furthermore, the GHRH-immunoreactivity in the area of ARC and median eminence decreased (Figure 6A, B), and GHRH mRNA expression in the ARC also decreased significantly in *Agrp Pdk1*$^{-/-}$ mice compared to *Agrp Cre* mice (Figure 6C).

3.4. Dominant-negative FoxO1 ameliorates short stature and reduced GH level in *Agrp Pdk1*$^{-/-}$ mice

We next examined a possible role of FoxO1 in linking PDK1 of AgRP neurons to bone metabolism. For this, transactivation-defective FoxO1 was introduced into *Agrp Pdk1*$^{-/-}$ mice by crossing *Agrp Δ256Foxo1* mice [21]. Body weight and food consumption were not significantly different between 6 week old female *Agrp Pdk1*$^{-/-}$ and *Agrp Pdk1*$^{-/-}$ *Δ256Foxo1* mice (Figure 7A,B). In *Agrp Pdk1*$^{-/-}$ *Δ256Foxo1* mice, femur length increased significantly compared with *Agrp Pdk1*$^{-/-}$ mice (Figure 7C,D). Furthermore, *Agrp Pdk1*$^{-/-}$ *Δ256Foxo1* mice exhibited significant restoration in a series of bone parameters compared with *Agrp Pdk1*$^{-/-}$ mice, which included cortical BMD, cancellous BMD, total BMD, minimum moment of inertia of area, and polar moment of inertia of area (Figure 7E–I). Moreover, in the *Agrp Pdk1*$^{-/-}$ *Δ256Foxo1* mice, serum GH concentration was significantly increased to a level that was to that in *Agrp Cre* mice (Figure 7J). Furthermore, daily urinary excretion of norepinephrine also increased

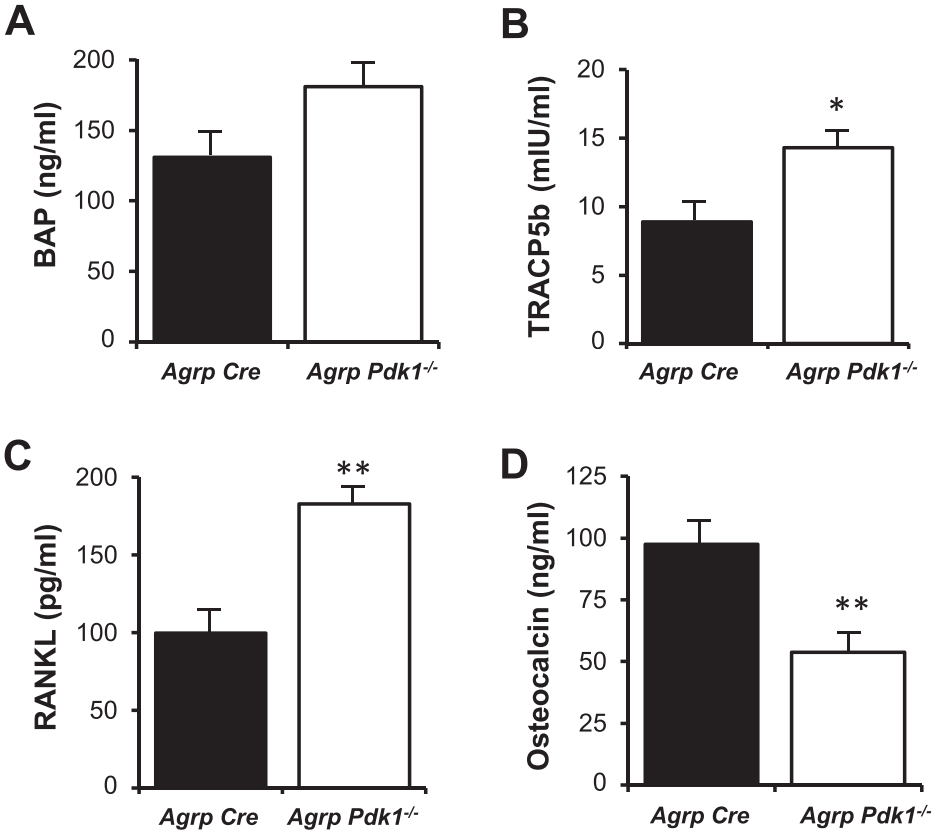

Figure 3: High turnover-type alteration of bone metabolism markers in *Agrp Pdk1*$^{-/-}$ mice. Plasma levels of bone-specific alkaline phosphatase (BAP) (A), tartrate-resistant acid phosphatase 5b (TRACP5b) (B), receptor activator of nuclear factor-κB ligand (RANKL) (C), and osteocalcin (D) in *Agrp Cre* and *Agrp Pdk1*$^{-/-}$ mice. n = 10–15 for each bar. $^{**}p < 0.01$, $^{*}p < 0.05$.

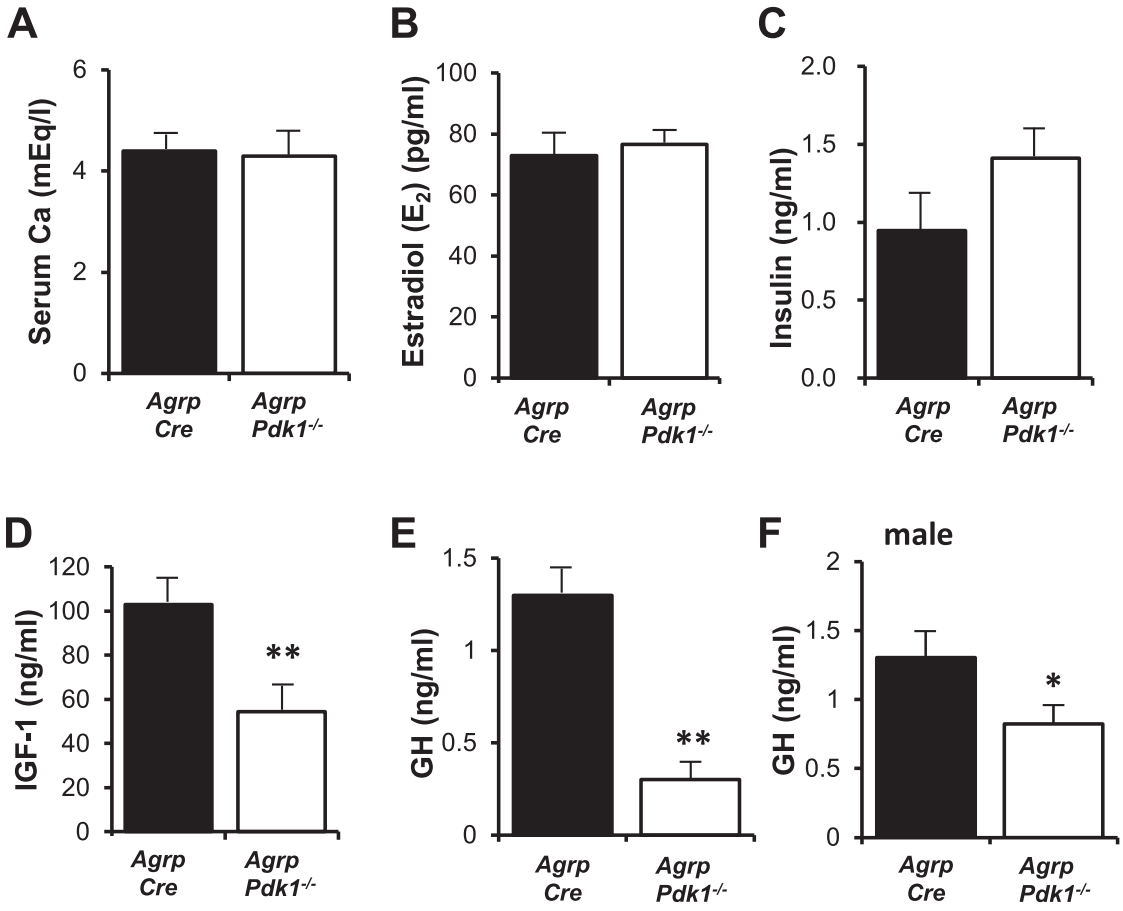

Figure 4: Plasma GH and IGF-1 levels are reduced in *Agrp Pdk1*$^{-/-}$ mice. Serum Ca^{2+} (**A**), plasma estradiol (E2) (**B**), and plasma insulin (**C**) in *Agrp Cre* and *Agrp Pdk1*$^{-/-}$ mice. Plasma levels of IGF-1 (**D**) and GH (**E**) were lower in female *Agrp Pdk1*$^{-/-}$ mice *than in* female *Agrp Cre*. **F**: Plasma level of GH was also lower in male *Agrp Pdk1*$^{-/-}$ mice. n = 10–15 for each bar. $^{**}p < 0.01$, $^{*}p < 0.05$.

in *Agrp Pdk1*$^{-/-}$ mice (Figure 7K). However, the increase in norepinephrine excretion was not attenuated by *Δ256Foxo1* expression (Figure 7K).

4. DISCUSSION

This study, for the first time, revealed that *Agrp Pdk1*$^{-/-}$ mice exhibit short stature, shortened limbs, and decreased bone density in both cortical and cancellous bones. The results indicate that PDK1 activity in ARC AgRP neurons plays a pivotal role in regulating bone metabolism. In *Agrp Pdk1*$^{-/-}$ mice, the GHRH-GH-IGF1 axis was markedly downregulated, which could serve as the mechanism underlying these changes of bone metabolism. Moreover, these bone metabolism disorders due to *Agrp Pdk1*$^{-/-}$ were rescued by additional expression of dominant negative FoxO1 in AgRP neurons. Shortened femoral length and decreased bone quantity were corrected, together with significant recovery of serum GH concentration. These results indicate that PDK1 regulates FoxO1 in AgRP neurons, and this neuronal signaling is linked to regulation of bone metabolism.

The main factors that influence the growth of long bones and bone remodeling are the mechanical stress from the burden of body weight and nutrition [31,32]. We previously reported that female *Agrp Pdk1*$^{-/-}$ mice, as were used in this study, showed decreases in body weight at 8 weeks of age and older [21]. However, in the present study using 6 week old female mice, no difference was observed in body weight and food consumption between *Agrp Pdk1*$^{-/-}$ mice, *Agrp Pdk1*$^{-/-}$ *Δ256Foxo1* mice, and *Agrp Cre* mice. It was also reported that the locomotor activity was similar between *Agrp Pdk1*$^{-/-}$ mice and *Agrp Cre* mice [21]. Accordingly, the influence of altered mechanical stress could be excluded.

Length from head to tail and femoral length were found to be significantly shorter in *Agrp Pdk1*$^{-/-}$ mice than *Agrp Cre* mice at 6 and 15 weeks of age. These phenotypes coincided with decreased plasma GH and IGF-1 levels and reduced GH mRNA expression in the pituitary. The results suggest that the bone abnormality in *Agrp Pdk1*$^{-/-}$ mice is caused by down regulation of the GH-IGF-1 system. This notion fits with the current view that the reduction in GH and IGF-1 from birth to adolescence impairs the ability of chondrocytes to ossify the epiphyseal plate, leading to reduced endochondral ossification and shortened limbs and trunk [33–36]. Furthermore, we found decreased mRNA expression of GHRH in the ARC of the *Agrp Pdk1*$^{-/-}$ mice, which may be responsible for the downregulation of the GH-IGF-1 axis. Hence, our results indicate that decreased activity of the GHRH-GH-IGF-1 axis serves as a primary cause for shortened limbs and delayed endochondral ossification in *Agrp Pdk1*$^{-/-}$ mice.

A link between AgRP neurons and the GHRH-GH-IGF-1 axis has also been found in larval teleosts. AgRP-immunoreactive nerve fibers directly project to the pituitary and coordinately regulate multiple endocrine axis including GH-IGF-1 axis, and the injection of AgRP-targeting antisense Morpholino oligonucleotides acutely suppresses

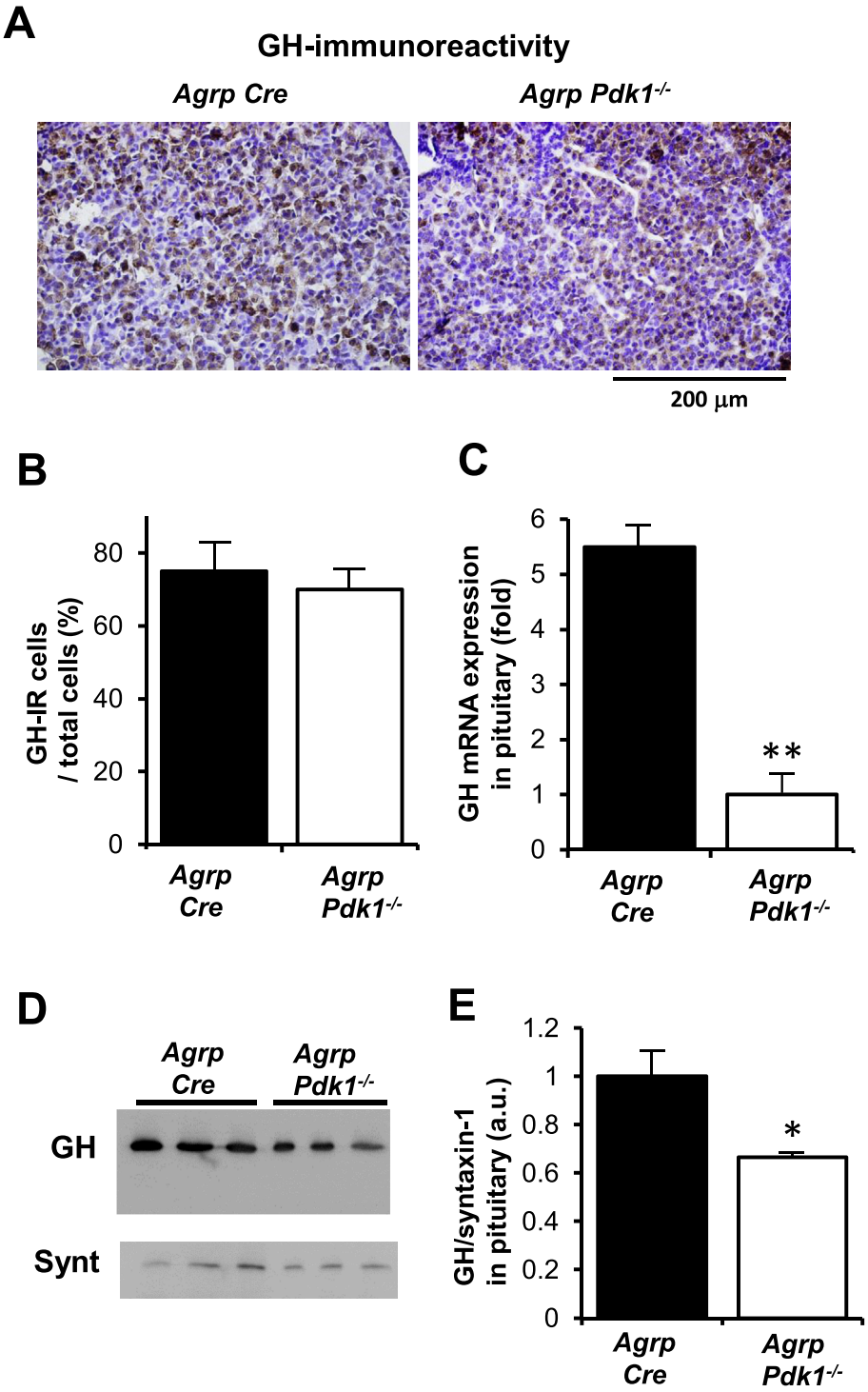

Figure 5: Expressions of GH protein and mRNA in pituitary are reduced in *Agrp Pdk1*$^{-/-}$ mice. A: Expression of GH by immunohistochemical staining in the anterior lobe of pituitary tissue of *Agrp Cre* and *Agrp Pdk1*$^{-/-}$ mice. Bar, 200 µm. **B:** The proportion of GH-immunoreactive (IR) cells to total cells in adenohypophysis. n = 3 per group. **C**: mRNA expression of GH in the pituitary of *Agrp Cre* and *Agrp Pdk1*$^{-/-}$ mice, determined by Real-time PCR. n = 5 per group. **D:** Western blot of GH and syntaxin-1 (synt) in the pituitary. **E**: Levels of GH protein relative to syntaxin-1 in the pituitary. n = 3 for each group. Bar represents mean ± s.e.m. *p < 0.05.

somatic growth and GH expression in pituitary in larval teleosts [22]. The central melanocortin system (AgRP/αMSH-MC4) coordinately regulates growth in teleosts.

Alternatively, NPY, the counterpart of AgRP in ARC neurons, could also be implicated in bone metabolism based on the following reports. Site-specific overexpression of NPY in the hypothalamus markedly reduces the capacity of osteoblasts to produce bone in mice [23]. The NPY Y2 receptor in hypothalamic neurons influences bone homeostasis [37]. GHRH neurons express the NPY Y2 receptor and are directly regulated by NPY [38]. NPY-immunoreactive fibers frequently form well-defined

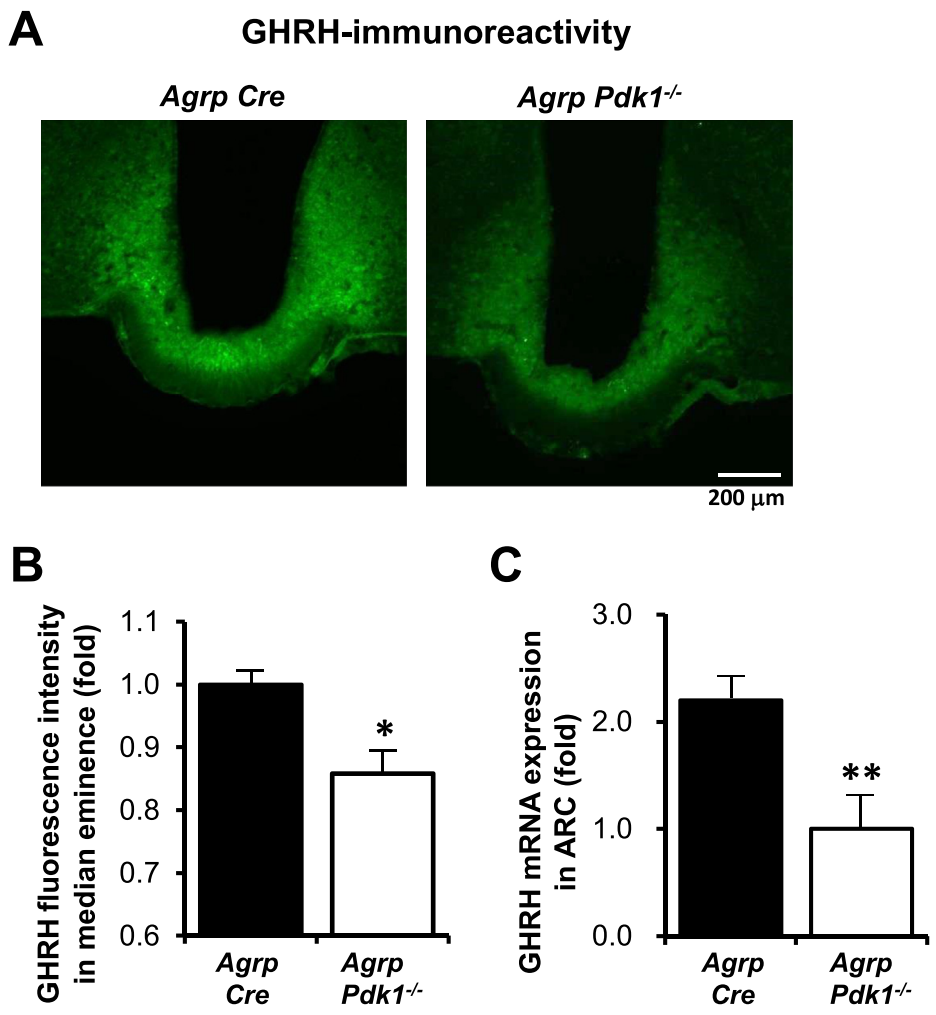

Figure 6: Expressions of GHRH protein and mRNA in hypothalamus are reduced in *Agrp Pdk1*$^{-/-}$ mice. A : Fluorescent immunostaining of GHRH in the hypothalamus of *Agrp Cre* mice and *Agrp Pdk1*$^{-/-}$ mice using rabbit anti-GHRH antibody and Alexa488-labeled second antibody. Bar, 200 μm. **B**: Relative fluorescent intensity of GHRH in the median eminence. n = 3 for each group. **C:** mRNA expression of GHRH in ARC of *Agrp Cre* and *Agrp Pdk1*$^{-/-}$ mice, determined by Real-time PCR. n = 5 per group. $^{**}p < 0.01$, $^{*}p < 0.05$.

fiber baskets around GHRH neurons [39]. Moreover, fasting-induced suppression of GHRH expression was blunted in the NPY−/− mouse, indicating that NPY is essential for the fasting-related regulation of GHRH [40]. Taken together, NPY in AgRP neurons may play a role in regulating bone metabolism. However, the mechanism that couples AgRP/NPY neurons to GHRH-GH system remains to be further elucidated.

In this study, short stature and lower plasma GH level in *Agrp Pdk1*$^{-/-}$ mice were more conspicuous in females than in males. The development of GHRH neurons depends on the sex and age [41]. Indeed, it was reported that the number of GHRH neurons is stabilized at 3 weeks of age in males, but still continue to increase in females [42]. Moreover, GHRH-stimulated GH secretion takes place in obese female but not male rats [43]. Furthermore, androgens stimulate bone remodeling in male mice during puberty [44]. These reports suggest the sex-dependent development of GHRH-GH-IGF-1 axis, which could be related to the remarkably short stature in female *Agrp Pdk1*$^{-/-}$ mice. The role of insulin as an anabolic agent has been established. The growth of mice lacking insulin receptor substrate-1 (IRS-1) was retarded after 15.5 embryonic days [45]. IRS-1−/− mice also exhibited low BMD with growth retardation [46]. Osteoblasts express functional insulin receptors, and mice lacking the insulin receptor in osteoblasts had reduced trabecular bone because of severely reduced number of osteoblasts, while showing normal longitudinal growth [47]. These reports suggest that insulin-IRS-1 signaling regulates the longitudinal growth by acting on cells other than osteoblasts. In IRS2 knockout mice, the compensatory increase of IRS1 in AgRP neurons led to less translocation of FOXO1 to the nucleus, thereby preventing hyperphagia and protecting from impaired glucose tolerance [48]. There is a possibility that insulin-IRS-1-FoxO1 signaling in AgRP neurons might regulate bone growth. The PDK1/FoxO1 pathway reportedly regulates food consumption and energy metabolism [18,49–51]. In AgRP neurons, activation of PDK1 suppresses FoxO1 to regulate energy homeostasis [21]. In the present study, we found that the inactivation of FoxO1 achieved in *Agrp Pdk1*$^{-/-}$ *Δ256Foxo1* mice rescued the impaired bone metabolism in *Agrp Pdk1*$^{-/-}$ mice, including short stature, shortened limbs, bone loss, and reduced plasma GH level. In addition, it was reported that the quantity of skeletal muscle was higher in 15 week old male *Agrp Pdk1*$^{-/-}$ *Δ256Foxo1* mice compared to *Agrp Pdk1*$^{-/-}$ mice [21]. Taken together, our results and those of others suggest that PDK1 to FoxO1 signaling in AgRP neurons serves to maintain the GHRH-GH-IGF1 axis

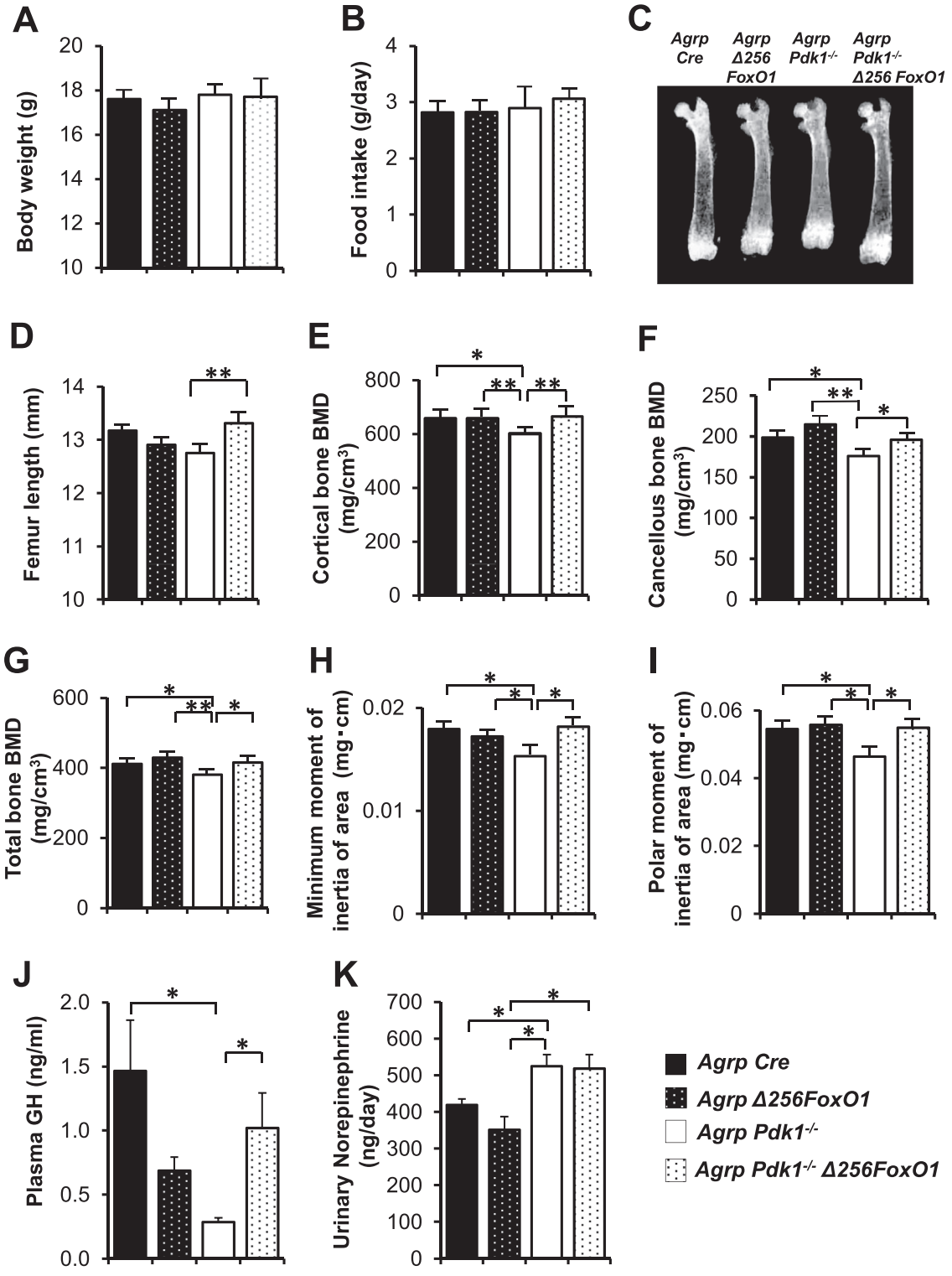

Figure 7: Disorders in bone metabolism and GH level are rescued by knockdown of Foxo1 in 6 week old female *Agrp Pdk1*$^{-/-}$ *Δ256Foxo1* mice. **A and B:** There were no significant differences in body weight and food intake between *Agrp Pdk1*$^{-/-}$ *Δ256Foxo1* mice and *Agrp Pdk1*$^{-/-}$ mice. **C and D:** Femur length in *Agrp Pdk1*$^{-/-}$ *Δ256Foxo1* mice was longer than that in *Agrp Pdk1*$^{-/-}$ mice and was comparable to that in *Agrp Δ256Foxo1* mice and *Agrp Cre* mice. **E-J**: Cortical bone BMD (E), cancellous bone BMD (F), total bone BMD (G), minimum moment of inertia of area (H), and polar moment of inertia of area (I) in *Agrp Pdk1*$^{-/-}$ *Δ256Foxo1* mice were greater than those in *Agrp Pdk1*$^{-/-}$ mice and were comparable to those in *Agrp Δ256Foxo1* mice and Cre mice. **J**: Plasma GH level was restored in *Agrp Pdk1*$^{-/-}$ *Δ256Foxo1* mice compared to *Agrp Pdk1*$^{-/-}$ mice. K: *Agrp Pdk1*$^{-/-}$ mice exhibited decreased urinary noradrenaline excretion, and this change was not altered by *Δ256Foxo1*. n = 10–23 per group. $^{**}p < 0.01$, $^{*}p < 0.05$.

and thereby promote the formation of both bone and skeletal muscle, a mechanism that supports locomotive activity. The present study has revealed a novel role of PDK1-FoxO1 signaling in AgRP neurons in regulating growth and locomotor functions, in addition to previously reported roles in regulating food consumption and energy metabolism. From nematodes to mammals, FoxO1 (DAF-16 in nematodes) is an important signaling molecule downstream of insulin/IGF-1 in various types of cells and is thought to be involved in the regulation of bone growth and lifespan [15]. The present study provided data to support that the activation of FoxO1 in AgRP neurons inhibits the GHRH-GH-IGF-1 axis. This finding suggests that the IGF-1/insulin-PDK1 cascade suppresses FoxO1 in AgRP neurons and consequently stimulates GHRH-GH-IGF-1 axis, forming a positive feedback loop for IGF-1 release. This mechanism could be implicated in the circadian pattern and surge of GH and IGF-1 release, which promotes growth during critical life periods. This study is the first demonstration, to the best of our knowledge, that FoxO1 in the central nervous system regulates the bone metabolism, though involvement of the osteoblast FoxO1 in bone quantity was previously reported [52,53].

The sympathetic nervous system is an important mediator of the brain control of bone metabolism [4,54]. Recently, Kim et al. reported that Sirt1 in AgRP neurons regulates bone mass via sympathetic nervous system [12]. In our study, urinary excretion of norepinephrine, which reflects sympathetic nervous system activity, was correlated with the bone phenotypes in *Agrp Pdk1*$^{-/-}$ *mice*. On the other hand, dominant negative FoxO1 attenuated the bone abnormality and GH-IGF-1 reduction witshout altering the urinary excretion of norepinephrine. These results suggest that the activation of the sympathetic nervous system does not serve as the major mediator for the impaired bone formation in *Agrp Pdk1*$^{-/-}$ *mice*, though it might be related to the overall regulation of bone metabolism. Instead, hypofunction of the GH-IGF-1 axis appears to be essential for the pathogenesis of growth retardation in *Agrp Pdk1*$^{-/-}$ *mice*. FoxO1 and Sirt1 in the hypothalamus reciprocally regulate the energy metabolism [55]. As the signaling molecule in AgRP neurons, Sirt1 is linked to stimulation, while FoxO1 is linked to inhibition, of bone formation.

This study provided evidence to support that the PDK1-FoxO1 signaling functions downstream of the PI3K/Akt pathway in ARC AgRP neurons and regulates bone metabolism. Together with the consensus that PI3K/Akt/PDK1/FoxO1 in ARC AgRP neurons is the major route through which insulin regulate feeding and energy metabolism, the PDK1-FoxO1 pathway in ARC AgRP neurons may provide a novel molecular target for treating osteoporosis, obesity and locomotive-metabolic syndrome.

ACKNOWLEDGMENTS

A part of this study was supported by Grant-in-Aid for Scientific Research (C) (24592277 and 15K09442) from JSPS to MN. This work was supported by Grant-in-Aid for Challenging Exploratory Research (26670453) from JSPS, the Ministry of Education, Culture, Sports, Science and Technology of Japan (MEXT)-Supported Programs for Strategic Research Foundation at Private Universities 2011–2015 and 2013–2017, a Grant-in-Aid from Health Labor Sciences Research Grants from the Ministry of Health, Labor, and Welfare, Japan, and a grant from Japan Diabetes Foundation to TY. This study was subsidized by JKA through its promotion funds from KEIRIN RACE to TY.

CONFLICT OF INTEREST

None declared.

REFERENCES

[1] Ahmed, L.A., Schirmer, H., Berntsen, G.K., Fønnebø, V., Joakimsen, R.M., 2006. Features of the metabolic syndrome and the risk of non-vertebral fractures: the Tromsø study. Osteoporosis International 17(3):426–432.

[2] Ducy, P., Amling, M., Takeda, S., Priemel, M., Schilling, A.F., Beil, F.T., et al., 2000. Leptin inhibits bone formation through a hypothalamic relay: a central control of bone mass. Cell 100(2):197–207.

[3] Takeda, S., Elefteriou, F., Levasseur, R., Liu, X., Zhao, L., Parker, K.L., et al., 2002. Leptin regulates bone formation via the sympathetic nervous system. Cell 111(3):305–317.

[4] Elefteriou, F., Ahn, J.D., Takeda, S., Starbuck, M., Yang, X., Liu, X., et al., 2005. Leptin regulation of bone resorption by the sympathetic nervous system and CART. Nature 434(7032):514–520.

[5] Wong, I.P., Nguyen, A.D., Khor, E.C., Enriquez, R.F., Eisman, J.A., Sainsbury, A., et al., 2013. Neuropeptide Y is a critical modulator of leptin's regulation of cortical bone. Journal of Bone and Mineral Research 28(4):886–898.

[6] Ollmann, M.M., Wilson, B.D., Yang, Y.K., Kerns, J.A., Chen, Y., Gantz, I., et al., 1997. Antagonism of central melanocortin receptors in vitro and in vivo by agoutirelated protein. Science 278(5335):135–138.

[7] Shutter, J.R., Graham, M., Kinsey, A.C., Scully, S., Luthy, R., Stark, K.L., 1997. Hypothalamic expression of ART, a novel gene related to agouti, is up-regulated in obese and diabetic mutant mice. Genes & Development 11(5):593–602.

[8] Beltramo, M., Campanella, M., Tarozzo, G., Fredduzzi, S., Corradini, L., Forlani, A., et al., 2003. Gene expression profiling of melanocortin system in neuropathic rats supports a role in nociception. Brain Research. Molecular Brain Research 118(1–2):111–118.

[9] Cowley, M.A., Pronchuk, N., Fan, W., Dinulescu, D.M., Colmers, W.F., Cone, R.D., 1999. Integration of NPY, AGRP, and melanocortin signals in the hypothalamic paraventricular nucleus: evidence of a cellular basis for the adipostat. Neuron 24(1):155–163.

[10] Cowley, M.A., Smart, J.L., Rubinstein, M., Cerdán, M.G., Diano, S., Horvath, T.L., et al., 2001. Leptin activates anorexigenic POMC neurons through a neural network in the arcuate nucleus. Nature 411(6836):480–484.

[11] Morton, G.J., Cummings, D.E., Baskin, D.G., Barsh, G.S., Schwartz, M.W., 2006. Central nervous system control of food intake and body weight. Nature 443(7109):289–295.

[12] Kim, J.G., Sun, B.H., Dietrich, M.O., Koch, M., Yao, G.Q., Diano, S., et al., 2015. AgRP neurons regulate bone mass. Cell Reports 13(1):8–14.

[13] Könner, A.C., Janoschek, R., Plum, L., Jordan, S.D., Rother, E., Ma, X., et al., 2007. Insulin action in AgRP-expressing neurons is required for suppression of hepatic glucose production. Cell Metabolism 5(6):438–449.

[14] Maejima, Y., Kohno, D., Iwasaki, Y., Yada, T., 2011. Insulin suppresses ghrelin-induced calcium signaling in neuropeptide Y neurons of the hypothalamic arcuate nucleus. Aging (Albany NY) 3(11):1092–1097.

[15] Salih, D.A., Brunet, A., 2008. FoxO transcription factors in the maintenance of cellular homeostasis during aging. Current Opinion in Cell Biology 20(2):126–136.

[16] Accili, D., Arden, K.C., 2004. FoxOs at the crossroads of cellular metabolism, differentiation, and transformation. Cell 117(4):421–426.

[17] Barthel, A., Schmoll, D., Unterman, T.G., 2005. FoxO proteins in insulin action and metabolism. Trends in Endocrinology and Metabolism 16(4):183–189.

[18] Lee, S.S., Kennedy, S., Tolonen, A.C., Ruvkun, G., 2003. DAF-16 target genes that control *C. elegans* life-span and metabolism. Science 300(5619):644–647.

[19] Hwangbo, D.S., Gershman, B., Tu, M.P., Palmer, M., Tatar, M., 2004. Drosophila dFOXO controls lifespan and regulates insulin signalling in brain and fat body. Nature 429(6991):562–566.

[20] Dong, X.C., Copps, K.D., Guo, S., Li, Y., Kollipara, R., DePinho, R.A., et al., 2008. Inactivation of hepatic FoxO1 by insulin signaling is required for adaptive nutrient homeostasis and endocrine growth regulation. Cell Metabolism 8(1):65–76.

[21] Cao, Y., Nakata, M., Okamoto, S., Takano, E., Yada, T., Minokoshi, Y., et al., 2011. PDK1-Foxo1 in agouti-related peptide neurons regulates energy homeostasis by modulating food intake and energy expenditure. PLoS One 6(4):e18324.

[22] Zhang, C., Forlano, P.M., Cone, R.D., 2012 Feb 8. AgRP and POMC neurons are hypophysiotropic and coordinately regulate multiple endocrine axes in a larval teleost. Cell Metabolism 15(2):256—264.

[23] Baldock, P.A., Sainsbury, A., Allison, S., Lin, E.J., Couzens, M., Boey, D., et al., 2005. Hypothalamic control of bone formation: distinct actions of leptin and y2 receptor pathways. Journal of Bone and Mineral Research 20(10):1851—1857.

[24] Huang, L., Tan, H.Y., Fogarty, M.J., Andrews, Z.B., Veldhuis, J.D., Herzog, H., et al., 2014. Actions of NPY, and its Y1 and Y2 receptors on pulsatile growth hormone secretion during the fed and fasted state. Journal of Neuroscience 34(49):16309—16319.

[25] Xu, A.W., Kaelin, C.B., Morton, G.J., Ogimoto, K., Stanhope, K., Graham, J., et al., 2005. Effects of hypothalamic neurodegeneration on energy balance. PLoS Biology 3(12):e415.

[26] Inoue, H., Ogawa, W., Asakawa, A., Okamoto, Y., Nishizawa, A., Matsumoto, M., et al., 2006. Role of hepatic STAT3 in brain-insulin action on hepatic glucose production. Cell Metabolism 3(4):267—275.

[27] Iskandar, K., Cao, Y., Hayashi, Y., Nakata, M., Takano, E., Yada, T., et al., 2010. PDK-1/Foxo1 pathway in POMC neurons regulates Pomc expression and food intake. American Journal of Physiology. Endocrinology and Metabolism 298(4):E787—E798.

[28] Shiraishi, A., Takeda, S., Masaki, T., Higuchi, Y., Uchiyama, Y., Kubodera, N., et al., 2000. Alfacalcidol inhibits bone resorption and stimulates formation in an ovariectomized rat model of osteoporosis: distinct actions from estrogen. Journal of Bone and Mineral Research 15(4):770—779.

[29] Hirata, M., Katsumata, K., Masaki, T., Koike, N., Endo, K., Tsunemi, K., et al., 1999. 22-Oxacalcitriol ameliorates high-turnover bone and marked osteitis fibrosa in rats with slowly progressive nephritis. Kidney International 56(6): 2040—2047.

[30] Parfitt, A.M., Drezner, M.K., Glorieux, F.H., Kanis, J.A., Malluche, H., Meunier, P.J., et al., 1987. Bone histomorphometry: standardization of nomenclature, symbols, and units. Report of the ASBMR Histomorphometry Nomenclature Committee. Journal of Bone and Mineral Research 2(6):595—610.

[31] Morey-Holton, E.R., Globus, R.K., 1998. Hindlimb unloading of growing rats; a model for predicting skeletal changes during space flight. Bone 22(5 Suppl): 83S—88S.

[32] Kappeler, L., De Magalhaes Filho, C., Leneuve, P., Xu, J., Brunel, N., Chatziantoniou, C., et al., 2009. Early postnatal nutrition determines somatotropic function in mice. Endocrinology 150(1):314—323.

[33] Pass, C., MacRae, V.E., Ahmed, S.F., Farquharson, C., 2009. Inflammatory cytokines and the GH/IGF-I axis: novel actions on bone growth. Cell Biochemistry and Function 27(3):119—127.

[34] Holmes, S.J., Economou, G., Whitehouse, R.W., Adams, J.E., Shalet, S.M., 1994. Reduced bone mineral density in patients with adult onset growth hormone deficiency. The Journal of Clinical Endocrinology & Metabolism 78(3):669—674.

[35] Ohlsson, C., Bengtsson, B.A., Isaksson, O.G., Andreassen, T.T., Slootweg, M.C., 1998. Growth hormone and bone. Endocrine Reviews 19(1):55—79.

[36] Ueland, T., 2004. Bone metabolism in relation to alterations in systemic growth hormone. Growth Hormone & IGF Research 14(6):404—417.

[37] Shi, Y.C., Lin, S., Wong, I.P., Baldock, P.A., Aljanova, A., Enriquez, R.F., et al., 2010. NPY neuron-specific Y2 receptors regulate adipose tissue and trabecular bone but not cortical bone homeostasis in mice. PLoS One 5(6):e11361.

[38] Lin, S., Lin, E.J., Boey, D., Lee, N.J., Slack, K., During, M.J., et al., 2007. Fasting inhibits the growth and reproductive axes via distinct Y2 and Y4 receptor-mediated pathways. Endocrinology 148(5):2056—2065.

[39] Deltondo, J., Por, I., Hu, W., Merchenthaler, I., Semeniken, K., Jojart, J., et al., 2008. Associations between the human growth hormone-releasing hormone- and neuropeptide-Y-immunoreactive systems in the human diencephalon: a possible morphological substrate of the impact of stress on growth. Neuroscience 153(4):1146—1152.

[40] Park, S., Peng, X.D., Frohman, L.A., Kineman, R.D., 2005. Expression analysis of hypothalamic and pituitary components of the growth hormone axis in fasted and streptozotocin-treated neuropeptide Y (NPY)-intact ($NPY^{+/+}$) and NPY-knockout ($NPY^{-/-}$) mice. Neuroendocrinology 81(6):360—371.

[41] Decourtye, L., Mire, E., Clemessy, M., Heurtier, V., Ledent, T., Robinson, I.C., et al., 2017. IGF-1 induces GHRH neuronal axon elongation during early postnatal life in mice. PLoS One 12(1):e0170083.

[42] McArthur, S., Robinson, I.C., Gillies, G.E., 2011. Novel ontogenetic patterns of sexual differentiation in arcuate nucleus GHRH neurons revealed in GHRH-enhanced green fluorescent protein transgenic mice. Endocrinology 152(2): 607—617.

[43] Cattaneo, L., De Gennaro Colonna, V., Zoli, M., Müller, E.E., Cocchi, D., 1999. Cocchi Hypothalamo—pituitary—IGF-1 axis in female rats made obese by overfeeding. Life Science 61(9):881—889.

[44] Venken, K., Movérare-Skrtic, S., Kopchick, J.J., Coschigano, K.T., Ohlsson, C., Boonen, S., et al., 2007. Impact of androgens, growth hormone, and IGF-I on bone and muscle in male mice during puberty. Journal of Bone and Mineral Research 22(1):72—82.

[45] Tamemoto, H., Kadowaki, T., Tobe, K., Yagi, T., Sakura, H., Hayakawa, T., et al., 1994. Insulin resistance and growth retardation in mice lacking insulin receptor substrate-1. Nature 372(6502):182—186.

[46] Ogata, N., Chikazu, D., Kubota, N., Terauchi, Y., Tobe, K., Azuma, Y., et al., 2000. Insulin receptor substrate-1 in osteoblast is indispensable for maintaining bone turnover. Journal of Clinical Investigation 105(7):935—943.

[47] Fulzele, K., Riddle, R.C., DiGirolamo, D.J., Cao, X., Wan, C., Chen, D., et al., 2010. Insulin receptor signaling in osteoblasts regulates postnatal bone acquisition and body composition. Cell 142(2):309—319.

[48] Burgos-Ramos, E., González-Rodríguez, A., Canelles, S., Baquedano, E., Frago, L.M., Revuelta-Cervantes, et al., 2012. Differential insulin receptor substrate-1 (IRS1)-related modulation of neuropeptide Y and proopiomelanocortin expression in nondiabetic and diabetic $IRS2^{-/-}$ mice. Endocrinology 153(3):1129—1140.

[49] Niswender, K.D., Morrison, C.D., Clegg, D.J., Olson, R., Baskin, D.G., Myers Jr., M.G., et al., 2003. Insulin activation of phosphatidylinositol 3-kinase in the hypothalamic arcuate nucleus: a key mediator of insulin-induced anorexia. Diabetes 52(2):227—231.

[50] Morrison, C.D., Morton, G.J., Niswender, K.D., Gelling, R.W., Schwartz, M.W., 2005. Leptin inhibits hypothalamic Npy and Agrp gene expression via a mechanism that requires phosphatidylinositol 3-OH-kinase signaling. American Journal of Physiology. Endocrinology and Metabolism 289(6):E1051—E1057.

[51] Kitamura, T., Feng, Y., Kitamura, Y.I., Chua Jr., S.C., Xu, A.W., Barsh, G.S., et al., 2006. Forkhead protein Foxo1 mediates Agrp-dependent effects of leptin on food intake. Nature Medicine 12(5):534—540.

[52] Ambrogini, E., Almeida, M., Martin-Millan, M., Paik, J.H., Depinho, R.A., Han, L., et al., 2010. Foxo-mediated defense against oxidative stress in osteoblasts is indispensable for skeletal homeostasis in mice. Cell Metabolism 11(2):136—146.

[53] Rached, M.T., Kode, A., Xu, L., Yoshikawa, Y., Paik, J.H., Depinho, R.A., et al., 2010. Foxo1 is a positive regulator of bone formation by favoring protein synthesis and resistance to oxidative stress in osteoblasts. Cell Metabolism 11(2):147—160.

[54] Yadav, V.K., Oury, F., Suda, N., Liu, Z.W., Gao, X.B., Confavreux, C., et al., 2009. A serotonin-dependent mechanism explains the leptin regulation of bone mass, appetite, and energy expenditure. Cell 138(5):976—989.

[55] Sasaki, T., Kim, H.J., Kobayashi, M., Kitamura, Y.I., Yokota-Hashimoto, H., Shiuchi, T., et al., 2010. Induction of hypothalamic Sirt1 leads to cessation of feeding via agouti-related peptide. Endocrinology 151(6):2556—2566.

